Mon. Not. R. Astron. Soc. **000**, 1–9 () Printed 4 September 2008 (MN LATEX style file v2.2)

SLAC-PUB-13382

# Mass models and environment of the new quadruply lensed quasar SDSS J1330+1810⋆

Masamune Oguri,[1]† Naohisa Inada,[2] Jeffrey A. Blackburne,[3] Min-Su Shin,[4] Issha Kayo,[5,6] Michael A. Strauss,[4] Donald P. Schneider,[7] and Donald G. York[8,9]

[1] *Kavli Institute for Particle Astrophysics and Cosmology, Stanford University, 2575 Sand Hill Rd., Menlo Park, CA 94025, USA.*
[2] *Cosmic Radiation Laboratory, RIKEN, 2-1 Hirosawa, Wako, Saitama 351-0198, Japan.*
[3] *Department of Physics, Massachusetts Institute of Technology and Kavli Institute for Astrophysics and Space Research, 70 Vassar St., Cambridge, MA, 02139, USA.*
[4] *Princeton University Observatory, Peyton Hall, Princeton, NJ 08544, USA.*
[5] *Institute for the Physics and Mathematics of the Universe, University of Tokyo, 5-1-5 Kashiwanoha, Chiba 277-8582, Japan.*
[6] *Department of Physics and Astrophysics, Nagoya University, Chikusa-ku, Nagoya 464-8602, Japan.*
[7] *Department of Astronomy and Astrophysics, Pennsylvania State University, 525 Davey Laboratory, University Park, PA 16802, USA.*
[8] *Department of Astronomy and Astrophysics, The University of Chicago, 5640 South Ellis Avenue, Chicago, IL 60637, USA.*
[9] *Enrico Fermi Institute, The University of Chicago, 5640 South Ellis Avenue, Chicago, IL 60637, USA.*

4 September 2008

**ABSTRACT**

We present the discovery of a new quadruply lensed quasar. The lens system, SDSS J1330+1810 at $z_s = 1.393$, was identified as a lens candidate from the spectroscopic sample of the Sloan Digital Sky Survey. Optical and near-infrared images clearly show four quasar images with a maximum image separation of $1\farcs76$, as well as a bright lensing galaxy. We measure a redshift of the lensing galaxy of $z_l = 0.373$ from absorption features in the spectrum. We find a foreground group of galaxies at $z = 0.31$ centred $\sim 120''$ southwest of the lens system. Simple mass models fit the data quite well, including the flux ratios between images, although the lens galaxy appears to be $\sim 1$ mag brighter than expected by the Faber-Jackson relation. Our mass modelling suggests that shear from nearby structure is affecting the lens potential.

**Key words:** gravitational lensing — quasars: individual (SDSS J133018.65+181032.1)

## 1 INTRODUCTION

Thus far about 100 gravitationally lensed quasars are known, of which $\sim 30$ are quadruple (four-image) lenses. The number ratio of quadruple lenses to double (two-image) lenses contains information on both the shapes of lensing galaxies and the luminosity function of source quasars (Rusin & Tegmark 2001; Chae 2003; Huterer et al. 2005; Oguri 2007b). In addition, quadruple lenses allow more detailed mass modelling of individual lenses. For instance, the larger number of images provides more constraints on the lens potential, which is essential in probing the effects of external perturbations on primary lenses (Keeton et al. 1997) and constraining the Hubble constant from time delay measurements (e.g., Suyu & Blandford 2006). Magnifications of merging image pairs in quadruple lenses satisfy distinct relations if the lens potential is smooth, but small-scale structures near the image can violate the relations. Thus flux ratios of quadruple lens images serve as unique probes of substructure in lens galaxies (Mao & Schneider 1998; Metcalf & Madau 2001; Chiba 2002; Dalal & Kochanek 2002; Schechter & Wambsganss 2002).

In this paper, we present the discovery of a new gravitationally lensed quasar with four lensed images, SDSS J133018.65+181032.1 (SDSS J1330+1810). It was discovered as part of the Sloan Digital Sky Survey Quasar Lens Search (SQLS; Oguri et al. 2006, 2008; Inada et al. 2008), which takes advantage of the large spectroscopic quasar catalog (see Schneider et al. 2007) of the Sloan Digital Sky Survey (SDSS; York et al. 2000) to locate new lensed quasars. We place particular emphasis on mass modeling and investigation of the structure around the lens.

The outline of this paper is as follows. We describe the

⋆ This paper includes data gathered with the 6.5 meter Magellan Telescopes located at Las Campanas Observatory, Chile. Based on observations obtained with the Apache Point Observatory 3.5-meter telescope, which is owned and operated by the Astrophysical Research Consortium. Use of the UH 2.2-m telescope for the observations is supported by NAOJ.
† E-mail: oguri@slac.stanford.edu



Published in the Monthly Notices of the Royal Astronomical Society
Work supported in part by US Department of Energy contract DE-AC02-76SF00515

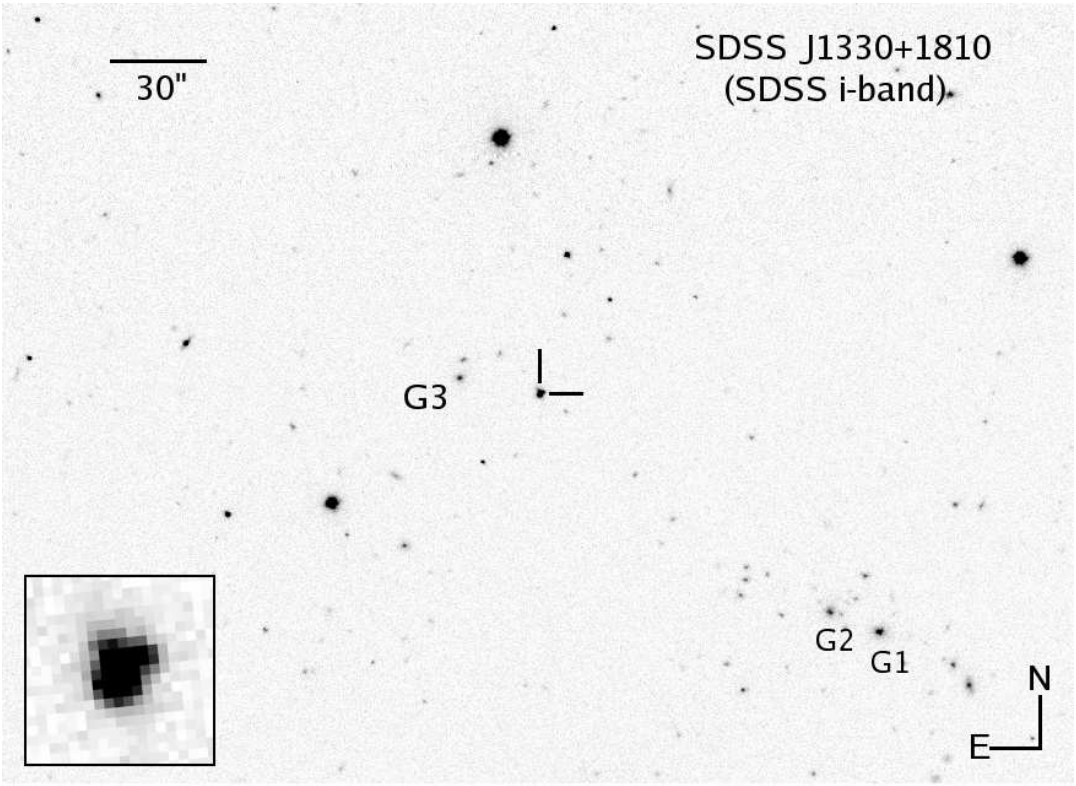


**Figure 1.** The SDSS $i$-band image of the SDSS J1330+1810 field. The pixel scale of the image is $0\farcs396$ pixel$^{-1}$, and the seeing was $1\farcs0$. The inset at lower left shows an expanded view of the lens system. Several bright galaxies in the field are indicated by G1-G3. The $i$-band Petrosian magnitudes of these galaxies (without correcting for Galactic extinction) are 17.72 (G1), 18.20 (G2), and 18.59 (G3).

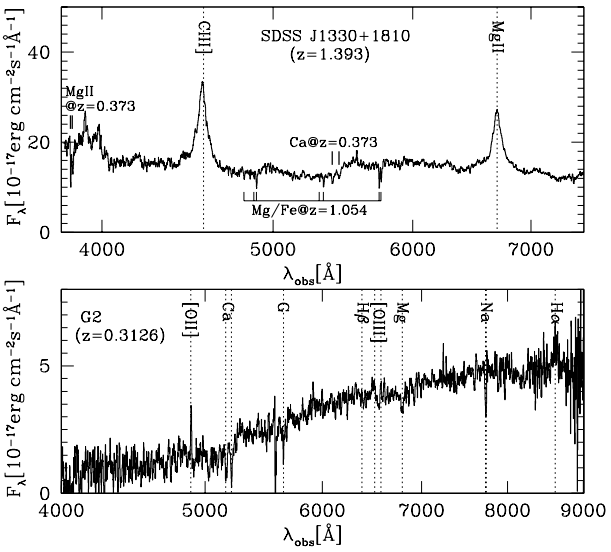


**Figure 2.** The SDSS spectra of SDSS J1330+1810 (*upper*) and the nearby galaxy G2 (*lower*). See Figure 1 for the relative positions. The spectral resolution is $R \sim 2000$, but the spectra are smoothed with a 5-pixel boxcar to suppress noise. Thick vertical line segments in the upper panel mark MgII and Ca absorption lines, which suggest the lens redshift of $z_l = 0.373$. A Mg/Fe absorption system at $z = 1.054$ is also shown by thin lines. The feature at $\sim 5600$Å in the spectrum of G2 is due to poor subtraction of a strong sky emission line (5575Å).

SDSS and follow-up data in Sections 2 and 3, respectively. The environment of the lens is discussed in Section 4. Section 5 is devoted to mass modelling. Our results are summarised in Section 6. Throughout the paper, we adopt the standard Lambda-dominated flat universe cosmology with matter density $\Omega_M = 0.26$ and the Hubble constant $h = 0.72$.

## 2 THE SDSS DATA

The lens system SDSS J1330+1810 was first identified in the data of the SDSS-II (Adelman-McCarthy et al. 2008). The SDSS-II is a survey to map 10,000 square degrees of the northern sky with a dedicated wide-field 2.5-meter telescope (Gunn et al. 2006) at the Apache Point Observatory in New Mexico, USA. It consists of a photometric survey (Gunn et al. 1998) with five broad-band optical filters (Fukugita et al. 1996) and a spectroscopic survey of quasars and galaxies selected by a series of target selection algorithms; Richards et al. (2002) present the SDSS quasar selection technique, and Blanton et al. (2003) describe the generation of the final SDSS spectroscopic targets. The homogeneity and good quality of the data, with an astrometric accuracy better than $0\farcs1$ rms per coordinate (Pier et al. 2003) and a photometric zeropoint accuracy better than 0.02 magnitude over the entire survey area (Hogg et al. 2001; Smith et al. 2002; Ivezić et al. 2004; Tucker et al. 2006; Padmanabhan et al. 2008), are essential for various statistical studies.

The SQLS identifies gravitationally lensed quasar can-

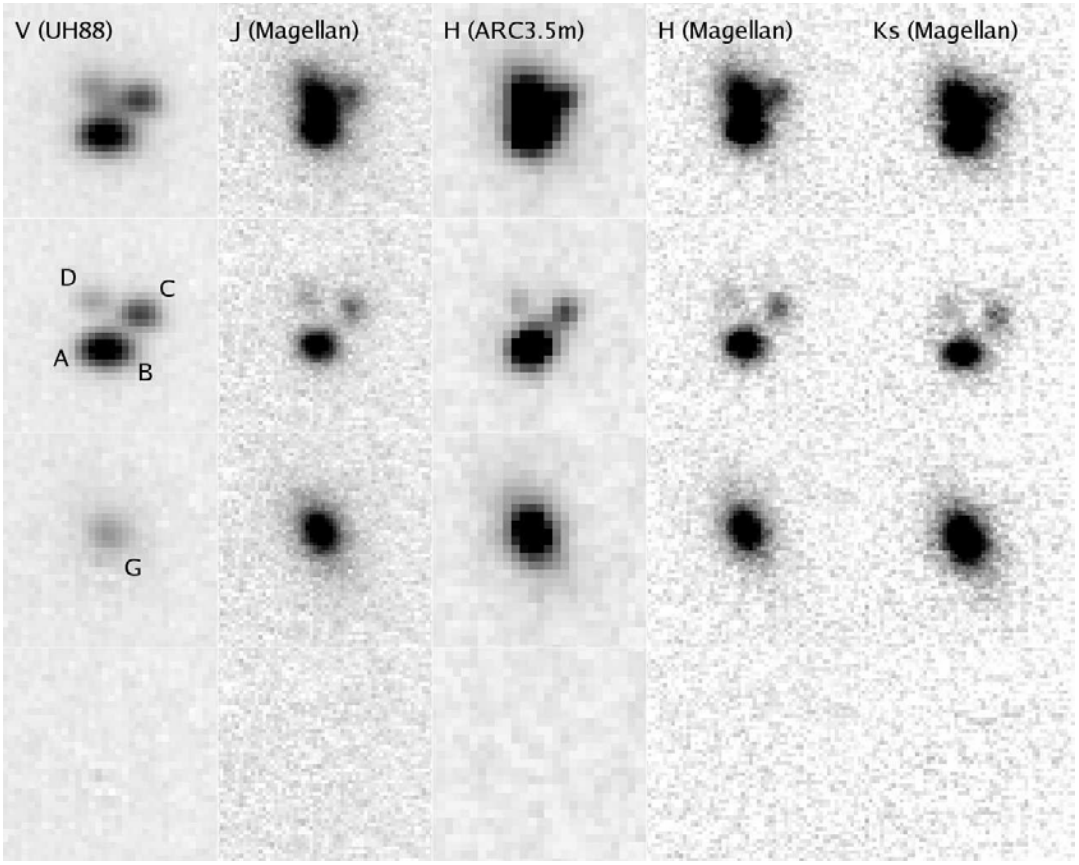


**Figure 3.** Images of SDSS J1330+1810. All the panels are $7'' \times 7''$ in size. North is up and East is left. The top row shows original follow-up images, the second row displays images after subtracting the lensing galaxy G1, the third row contains images after subtracting 4 PSFs (quasar images), and the bottom row shows the results after subtracting the galaxy and all four quasar components.

**Table 1.** Relative astrometry and photometry from the follow-up images (see Figure 3). The positive directions of $x$ and $y$ are North and West, respectively. The J2000 coordinates of component A are (RA, Dec) = (202.5778, 18.1756). The positional errors are estimated from the scatter between the five follow-up images.The errors on the magnitudes are statistical errors only and do not include systematic errors coming from uncertainties of PSFs and the galaxy profile. The magnitudes have not been corrected for Galactic extinction.

| Name | $x$ [arcsec] | $y$ [arcsec] | $V$ (UH88) [mag] | $J$ (Magellan) [mag] | $H$ (ARC3.5m) [mag] | $H$ (Magellan) [mag] | $K_s$ (Magellan) [mag] |
|---|---|---|---|---|---|---|---|
| A | $\equiv 0$ | $\equiv 0$ | $19.02 \pm 0.02$ | $18.36 \pm 0.05$ | $17.32 \pm 0.05$ | $17.40 \pm 0.07$ | $17.06 \pm 0.04$ |
| B | $0.42 \pm 0.03$ | $-0.01 \pm 0.03$ | $19.72 \pm 0.03$ | $18.68 \pm 0.07$ | $17.54 \pm 0.06$ | $17.73 \pm 0.09$ | $17.30 \pm 0.05$ |
| C | $1.30 \pm 0.03$ | $1.19 \pm 0.03$ | $19.89 \pm 0.01$ | $19.12 \pm 0.02$ | $18.18 \pm 0.02$ | $18.24 \pm 0.02$ | $17.90 \pm 0.03$ |
| D | $-0.24 \pm 0.04$ | $1.58 \pm 0.04$ | $21.45 \pm 0.04$ | $19.83 \pm 0.05$ | $19.36 \pm 0.12$ | $19.13 \pm 0.05$ | $18.62 \pm 0.06$ |
| G | $0.24 \pm 0.03$ | $0.97 \pm 0.03$ | $19.48 \pm 0.04$ | $16.77 \pm 0.01$ | $16.00 \pm 0.01$ | $16.08 \pm 0.02$ | $15.26 \pm 0.01$ |

didates using a well-defined algorithm (Oguri et al. 2006) applied to the spectroscopic SDSS quasars. The algorithm has two parts: morphological selection, which identifies quasars that are poorly fitted by the Point Spread Function (PSF), and colour selection, which examines objects near each spectroscopic quasar and selects those with colours similar to the quasar as lens candidates. These two selections are designed to locate small- ($\sim 1''$) and large-separation ($\gtrsim 3''$) lensed quasars, respectively. The SQLS has already discovered $> 20$ new gravitationally lensed quasars from the SDSS data using this algorithm, including both double and quadruple lenses (e.g., Kayo et al. 2007, and references therein).

The gravitational lens SDSS J1330+1810 was selected as a lens candidate by the morphological selection algorithm.[1] Figure 1 shows the SDSS $i$-band image of the system (seeing of $1\farcs0$). The enlarged image clearly indicates that the system, which is classified as a quasar at $z = 1.393$ from the SDSS spectrum (see Figure 2), is not a point source but consists of multiple components. The morphology of the quasar in the SDSS image is similar to that of SDSS J0924+0219 (Inada et al. 2003), suggesting that this is likely to be a

[1] The SDSS photometric designation of SDSS J1330+1810 is 5308/40/1/73/88 (run/rerun/camcol/filed/ID), and the spectroscopic designation is 2641/255/54230 (plate/fiber/MJD).

fold-type quadruple lens. In the SDSS spectrum we find absorption lines at $\sim$ 3850Å and $\sim$ 5400Å, consistent with MgII and Ca lines due to a galaxy at $z = 0.373$. We interpret these features as absorptions by the lensing galaxy. In addition a Mg/Fe absorption system at $z = 1.054$ is seen in the spectrum. Since its redshift is quite close to the source redshift, the effect of the absorber at $z = 1.054$ on the lens potential is expected to be small.

The SDSS image shows a concentration of red galaxies $\sim 120''$ southwest of SDSS J1330+1810 (see Figure 2, around G1 and G2). One of the galaxies, G2, was targeted by the luminous red galaxy program (Eisenstein et al. 2001) and has been observed spectroscopically in the SDSS (Figure 2), with a redshift of $z = 0.3126$. The presence of the [OII] emission line (rest-frame equivalent width of $-9$Å) suggests ongoing star formation activity in galaxy G2. We explore the possible group further in Section 4.

## 3 FOLLOWUP OBSERVATIONS

### 3.1 Optical and Near-Infrared Imaging

Near-infrared ($JHK_s$-bands) images were taken using Persson's Auxilliary Nasmyth Infrared Camera (PANIC; Martini et al. 2004) at the 6.5-meter Magellan I (Walter Baade) telescope on 2007 July 5. The total exposure time was 405 sec in $J$, 540 sec in $H$, and 360 sec in $K_s$. The seeing was $0\farcs74 - 0\farcs82$. We also obtained $H$-band images with the Near-Infrared Camera and Fabry-Perot Spectrometer (NICFPS) at the Astrophysical Research Consortium 3.5-meter (ARC3.5m) Telescope on 2007 June 1. The total exposure time was 1200 sec and the seeing was $0\farcs88$. Optical imaging was conducted with the Tektronix 2048x2048 CCD camera at the University of Hawaii 2.2-meter (UH88) telescope. A 500 sec image in $V$-band was taken on 2008 March 6, under $0\farcs81$ seeing. All the data were reduced using standard IRAF tasks. The zero-point magnitudes of the infrared images were estimated using Two Micron All Sky Survey (2MASS) data (Skrutskie et al. 2006), whereas the UH88 image was calibrated by the standard star PG0918+029 (Landolt 1992).

The images shown in Figure 3 confirm that the system is indeed a typical fold-type quadruple lens, with two merging images and the other two images on the other side of the lens. For definiteness, we fit the images using GALFIT (Peng et al. 2002). The assumed model consists of four PSFs and a lens galaxy modelled by a Sersic profile with the convolution of the PSF. We adopt nearby stars as PSF templates. We first left the Sersic index $n$ as a free parameter and found the best-fit value to be $n \approx 3.4$, which is close to the canonical value for early type galaxies, $n = 4$. Thus in what follows we fix the Sersic index to $n = 4$. We find that this model fits the data quite well. The subtracted images shown in Figure 3 show virtually no residuals. Table 1 summarises the relative astrometry and photometry from the fitting. Following convention, we name four quasar components A-D, in decreasing order of their brightnesses, and we name the lensing galaxy G. The relative positions of the four components agree well among the high angular resolution images, with a scatter of $\sim 0\farcs03$. The maximum separation between images is $1\farcs76$. For the NIR images, the lensing galaxy is modelled well by the Sersic profile ($n = 4$) with scale radius $R_e \sim 0\farcs7 - 0\farcs9$, ellipticity $e \sim 0.57$, and position angle (East of North) $\theta_e \sim 24^\circ$. The lensing galaxy has somewhat different best-fit scale radius and ellipticity in the UH88 $V$-band image, $R_e \sim 1\farcs42$ and $e \sim 0.28$.

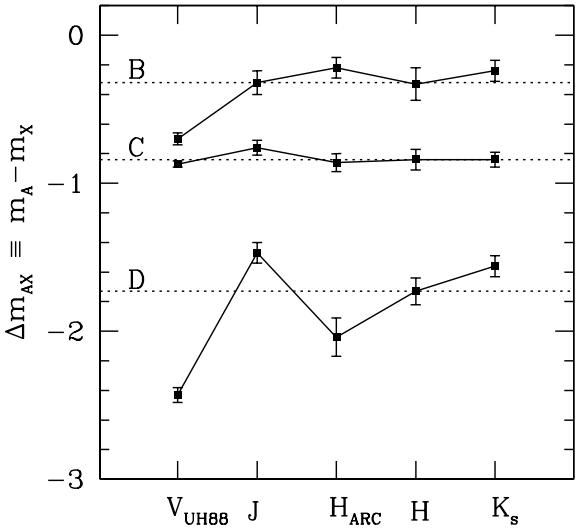


**Figure 4.** Flux ratios of quasar images from the follow-up images (see also Figure 3 and Table 1). We plot magnitude differences between images B-D and the brightest image A, $\Delta m \equiv m_A - m_X$ ($X = B - D$). Dotted horizontal lines indicate median values of individual ratios, which we adopt for mass modelling.

In Figure 4, we compare the flux ratios of the quasar images derived from the five follow-up images. They are broadly consistent between different wavelengths, which further supports the lensing interpretation. However, there are some noticeable differences in flux ratios, in particular those in the UH88 $V$-band. While additional systematic errors associated with image fitting might account for the differences, a possible physical interpretation is differential dust extinction which is commonly seen in lensed quasar systems (e.g., Falco et al. 1999); this helps to explain the different $V$-band flux ratios from those in NIR images, because the effect of dust is much more pronounced in $V$-band than in NIR. The $V$-band image was taken $8-9$ months after the observations in near-infrared, and thus time variability (intrinsic and/or due to microlensing) of the quasar images might also contribute to the differences. Additional imaging observations in the same and different bands will help to distinguish these possibilities.

We note that the case for gravitational lensing is already very strong from its characteristic configuration of image components, the similarity of their colors, and the presence of a bright lensing galaxy. However, the ultimate confirmation of its lensing nature will require the spectroscopy of all image components to show they have similar spectral features.

### 3.2 Optical Spectroscopy

We conducted spectroscopy of the system with the Dual Imaging Spectrograph (DIS) at the ARC3.5m telescope on 2008 June 6. We used a $1\farcs5$ slit and the gratings of B400

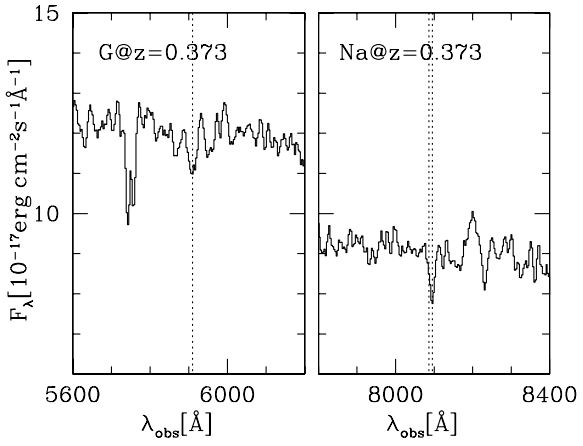


**Figure 5.** G-band (*left*) and Na (*right*) absorption lines of the lensing galaxy at $z = 0.373$ from the spectrum of SDSS J1330+1810 obtained with the DIS at the ARC3.5m telescope. The feature at 5750Å is an MgII doublet at $z = 1.054$ (see also Figure 2).

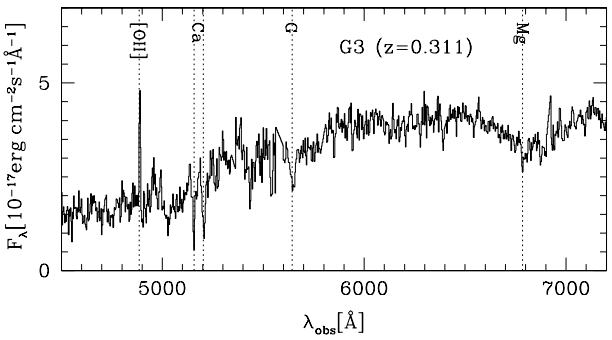


**Figure 6.** The spectrum of galaxy G3 (See Figure 1) taken with the DIS at the ARC3.5m telescope.

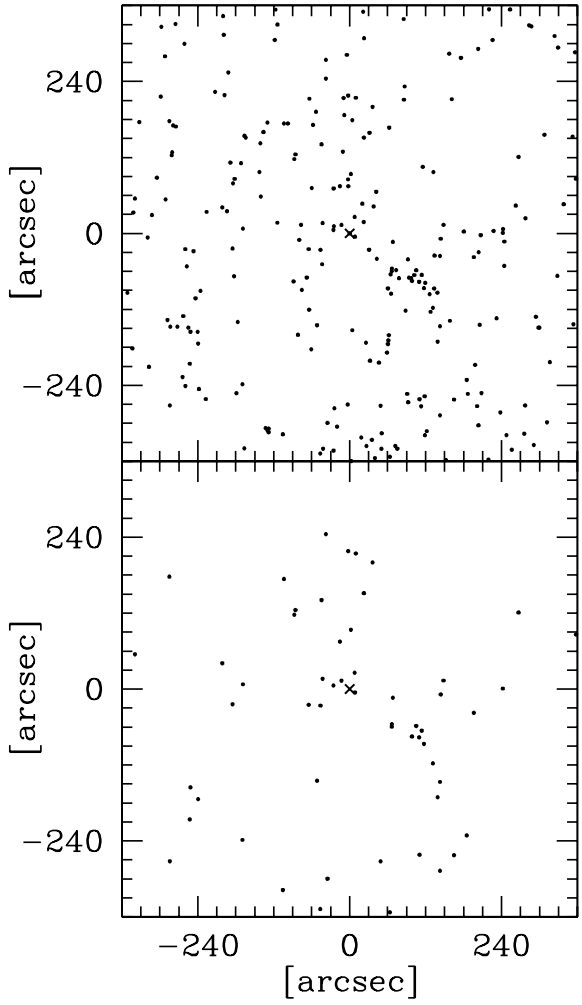


**Figure 7.** *Upper:* The spatial distribution of all the SDSS galaxies brighter than $i = 21$ in the vicinity of the lens at (0, 0). North is up and East is left. The position of the lens system is indicated by a cross. *Lower:* The spatial distribution of galaxies whose photometric redshifts are consistent with $z = 0.31$.

(disperison of 1.8Å) in the blue channel and R300 (2.3Å) in the red channel. The slit was aligned to observe nearby galaxy G3 (see Figure 1) and SDSS J1330+1810 simultaneously. The spectral resolution is $R \sim 500$. We obtained the spectrum of the Northern-half of SDSS J1330+1810 (around image C and D) where the relative contribution of galaxy G to the flux is much stronger; however, because of poor seeing ($\sim 1\farcs2$), we could not separate components C, D, and G. The exposure time was 2400 sec. The data were reduced using standard IRAF tasks.

This spectrum shows a weak absorption line at $\sim 5900$Å and moderate absorption line at $\sim 8100$Å (Figure 5), in excellent agreement with those of the G-band 4304Å absorption and Na 5889/5896Å absorption doublet redshifted to $z = 0.373$, the lens redshift inferred from absorption lines in the SDSS spectrum (see Figure 2). Since these absorptions are weak, they were not seen in the SDSS spectrum. We note that the DIS spectrum exhibits clear emission lines of quasars, which should originate both from images C/D and from scattered fluxes from images A/B.

The redshift of galaxy G3 is $z = 0.311$ (Figure 6), which is quite close to the redshift of galaxy G2, $z = 0.3126$. The two galaxies have similar spectra, with significant [OII] emission of the same rest-frame equivalent width. The 4000Å break of G3 is weaker than that of G2, which implies that star formation happened more recently in G3.

## 4 ENVIRONMENT OF THE LENS GALAXY

The wide-field image suggests a possible group of galaxies located near the lens system (see Section 2). The high incidence of groups near strong lens systems has been noted before (Fassnacht & Lubin 2002; Momcheva et al. 2006; Williams et al. 2006; Auger et al. 2007; Cabanac et al. 2007; Shin et al. 2008; Treu et al. 2008) and is theoretically expected (Keeton et al. 2001; Oguri et al. 2005). Although the redshift of the possible group, $z = 0.31$, differs from the lens redshift $z_l = 0.373$, a foreground group affects the lens po-

tential in a similar way as does a group at the same redshift.[2] In this section, we study the distribution and properties of galaxies in the field from the SDSS.

First we extract locations and brightnesses of galaxies in the $12' \times 12'$ field centred on the lens system from the SDSS data release 6 (DR6; Adelman-McCarthy et al. 2008). We adopt the Petrosian (1976) magnitudes in what follows. We restrict our analysis to galaxies brighter than $i = 21$, where star-galaxy separation is reliable. To study the distribution at $z \sim 0.31$, we adopt photometric redshift measurement in the SDSS databases (Csabai et al. 2003; Adelman-McCarthy et al. 2007). Specifically, we select galaxies whose photometric redshifts are consistent with $z = 0.31$ within their quoted errors. Therefore our study here is not necessarily restricted to red elliptical galaxies but includes blue galaxies as well. Galaxies with large photometric redshift errors, $\Delta z > 0.2$, are are excluded from our analysis.

We show the angular distributions of all galaxies and galaxies at $z \sim 0.31$ in Figure 7. There is a clear concentration of galaxies to the southwest of the lens. The structure is more pronounced after applying a cut by the photometric redshift. We note that G1 is the brightest among galaxies at $z \sim 0.31$ selected in this way. Together with the agreement of the spectroscopic redshifts of G2 and G3 (Sections 2 and 3.2), we conclude that there is a foreground group of galaxies at $z \sim 0.31$ with its centre $\sim 120''$ southwest of the lens system (corresponding to transverse physical distances of $390h^{-1}$kpc at $z = 0.31$ and $440h^{-1}$kpc at $z = 0.373$), centred around G1 and G2. It is worth noting that a concentration of galaxies can also be seen around G3, which suggests that there might be a sub-clump of the group around G3.

There is a possibility that a concentration of galaxies at the lens redshift $z = 0.373$ exists in additional to the group at $z = 0.31$. However, most of galaxies examined here are rather faint and have large errors on the photometric redshifts, which prevent us to distinguish structures at $z = 0.31$ from $z = 0.373$. Additional imaging and spectroscopic follow-up observations are necessary to explore this issue further.

## 5 MASS MODELLING

We constrain the lens potential of this system using the observed image positions and flux ratios. The relative positions of the quasar images and galaxies and their errors are adopted from Table 1. Flux ratios are estimated from the median of the measurements in the five follow-up images (see Figure 4). Considering the scatter, we assume a conservative error on the magnitude difference between quasar images, $\sigma(\Delta m) = 0.2$. We adopt two standard mass models that are widely used in modelling strong lens systems; a Singular Isothermal Ellipsoid (SIE) and an SIE plus external shear perturbation (SIEx). Since it is of interest whether the models can explain the observed flux ratios or not, for each model we consider two cases; one includes flux ratios as observational constraints and the other only uses relative positions as constraints. The optimisation of model parameters is performed using a software package called *glafic* (M. Oguri, in preparation).

[2] From the discussion of Keeton (2003), it is estimated that a weak foreground external shear $\gamma$ at $z = 0.31$ is equivalent to an external shear of $\approx 0.8\gamma$ at $z = 0.373$.

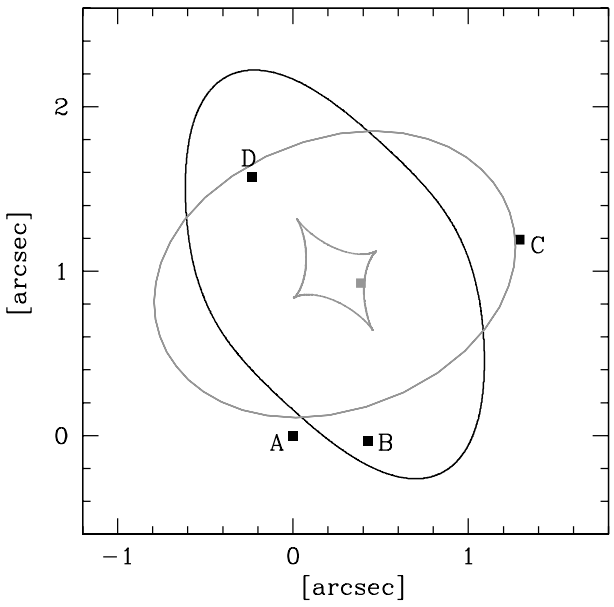


**Figure 8.** The best-fit model (SIEx, flux ratios are included as constraints) is shown. See Table 2 for best-fit parameters. The black curve and squares indicate the critical curve of the best-fit model and the predicted image positions. Observed image positions are within the symbols. Grey curves and the square are the corresponding caustics and source position.

Best-fit $\chi^2$ and model parameters are summarised in Table 2. We find that all four models considered here produce reasonably good fits to the data ($\chi^2/\mathrm{dof} \lesssim 1$). The models successfully fit the flux ratios, therefore this lens system does not exhibit any sign of flux ratio anomaly. Moreover, the flux ratios predicted by models with no flux ratio constraints broadly agree with observed flux ratios. The successful mass modeling further supports the lensing nature of this system. We show the critical curve and caustics for the best-fit model (SIEx with flux ratios as constraints) in Figure 8, which indicates that images B and D are saddle-point images and images A and C are minima. Given the best-fit mass models, we can predict time delays between the images. Assuming that the lensing galaxy is located at $z_l = 0.373$, for each best-fit model we compute time delays between image A and the other images, which are listed in Table 2. Time delays are rather model dependent, particularly for $\Delta t_{AB}$ and $\Delta t_{AC}$, for which the maximum fractional differences between different models are $\gtrsim 70\%$. This is because shorter time delays are more easily affected by perturbations in the primary lens potential (Oguri 2007a).

The large ellipticities of $0.31 - 0.56$ in the best-fit models are broadly consistent with the observed shape of the lensing galaxy (see Section 3.1). We find that the best-fit position angle of the galaxy, $\theta_e$, is different between models with and without external shear: $\theta_e \sim 34^\circ$ when the external shear is not included, whereas $\theta_e \sim 25^\circ$ for models including external shear. The observed position angle of galaxy G, $\theta_e = 24^\circ \pm 2^\circ$, agrees very well with the latter, suggesting the non-negligible effect of external shear on the lens poten-

**Table 2.** Best-fit mass models of SDSS J1330+1810. The column 'Flux' shows whether flux ratios are included as constraints or not. The parameter $\theta_{\rm Ein}$, $e$, and $\gamma$ denote the Einstein radius, ellipticity, and external shear, respectively. The position angle of ellipticity and shear, $\theta_e$ and $\theta_\gamma$, are measured East of North. $\chi^2_{\rm pos}$, $\chi^2_{\rm gal}$, and $\chi^2_{\rm flux}$, indicate chi-square values from image positions, lens galaxy positions, and flux ratios. The total chi-square $\chi^2$ is the sum of these three. Also shown are time delays between images predicted by the best-fit models, adopting the lens redshift $z_l = 0.373$.

| Model | Flux | $\chi^2$/dof | $\chi^2_{\rm pos}$ | $\chi^2_{\rm gal}$ | $\chi^2_{\rm flux}$ | $R_{\rm Ein}$ | $e$ | $\theta_e$[deg] | $\gamma$ | $\theta_\gamma$[deg] | $\Delta t_{AB}$[day] | $\Delta t_{AC}$[day] | $\Delta t_{AD}$[day] |
|---|---|---|---|---|---|---|---|---|---|---|---|---|---|
| SIE | No | 2.10/3 | 2.10 | 0.01 | ··· | 0.″97 | 0.31 | 34 | ··· | ··· | −0.15 | 6.04 | −11.68 |
| SIE | Yes | 7.28/6 | 2.80 | 0.01 | 4.47 | 0.″97 | 0.32 | 34 | ··· | ··· | −0.18 | 5.91 | −11.83 |
| SIEx | No | 0.33/1 | 0.13 | 0.21 | ··· | 0.″97 | 0.39 | 25 | 0.05 | −88 | −0.20 | 6.76 | −12.17 |
| SIEx | Yes | 1.14/4 | 0.76 | 0.13 | 0.25 | 0.″99 | 0.56 | 25 | 0.11 | −75 | −0.31 | 10.28 | −12.69 |

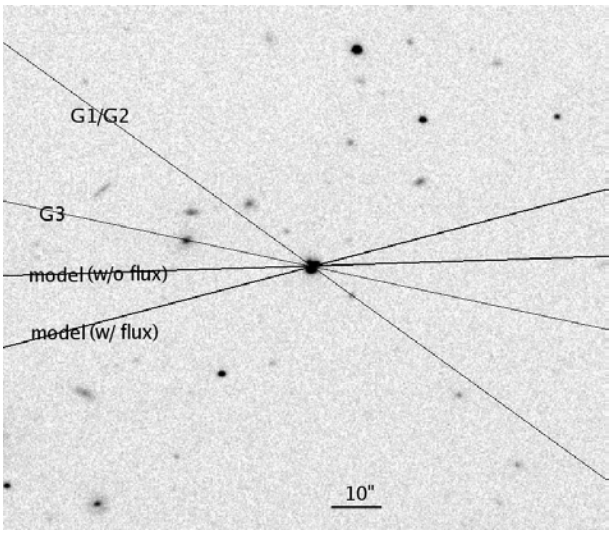


**Figure 9.** The UH88 $V$-band image around the lens system. North is up and East is left. Shear directions in our best-fit models ($\theta_\gamma = -88°$ for the model without flux constraints, and $-75°$ for the model with flux constraints) are shown by thick solid lines. Directions to a nearby bright galaxy (G3) and the centre of the group (G1/G2) are indicated by thin solid lines.

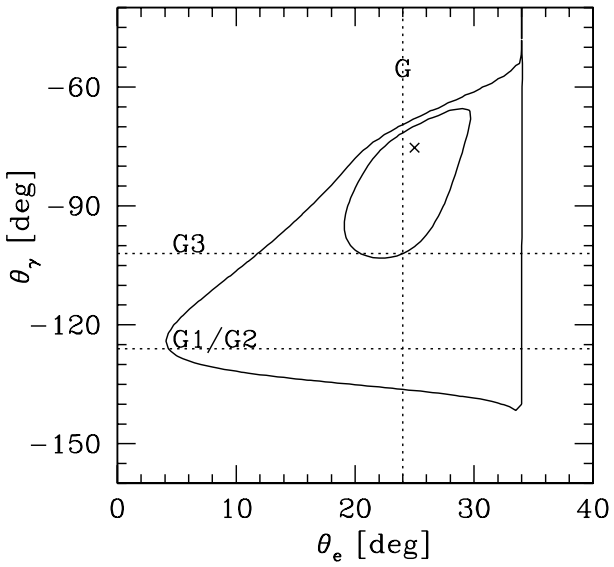


**Figure 10.** $1\sigma$ and $2\sigma$ contours of the position angles of the ellipticity and external shear for the SIEx model. Flux ratios are included as constraints. The cross indicates the best-fit values (see Table 2). The vertical dotted line indicates the observed orientation of the lensing galaxy. Horizontal dotted lines are expected values (see also Figure 9) when the external perturbations are caused by the centre of the group (G1/G2) or the nearby bright galaxy (G3).

tial, as in other quadruple lens systems (Keeton et al. 1997). However, there is no obvious perturber along the shear direction, $\theta_\gamma = -88°$ or $-75°$ (see Figure 9). Thus in Figure 10 we present likelihood contours in the $\theta_e$-$\theta_\gamma$ plane. Specifically, for each ($\theta_e$, $\theta_\gamma$) we perform $\chi^2$ minimisations and use $\Delta\chi^2$ to draw contours at the $1\sigma$ and $2\sigma$ confidence levels. We find that the shear direction to galaxy G3 is consistent with the observations at the $1\sigma$ level. The resultant ellipticity position angle is $20° \lesssim \theta_e \lesssim 24°$ and is also consistent with the observed orientation of the lensing galaxy. On the other hand, the shear direction to galaxies G1 and G2 fails to fit the data at the $\sim 2\sigma$ level. Therefore we conclude that nearby galaxy G3, rather than the group of galaxies $\sim 120''$ southwest of the lens, is likely to be the main perturber to the lens system.

Although the shear amplitudes of $0.05 - 0.1$ are slightly larger than would be produced by a single galaxy $\sim 30''$ away from the lens, the existence of the group suggests that dark matter sufficient to produce the shear amplitudes can be associated with galaxy G3. This idea is supported by an apparent concentration of galaxies at $z \sim 0.31$ around G3 (see Figure 7).

Given the best-fit Einstein radius $R_{\rm Ein} = 0.''97$, we can compute magnitudes of the lensing galaxy expected from the Faber-Jackson relation (Faber & Jackson 1976), adopting the model of Rusin et al. (2003). From the lens redshift $z_l = 0.373$, the apparent magnitudes are predicted to be $V = 20.7$, $J = 17.9$, $H = 16.7$ and $K_s = 16.1$, which are $0.7 - 1.2$ mag fainter than the observed magnitudes of the lensing galaxy. Using the same model, we find that the observed magnitudes correspond to the lens redshift of $z_l \sim 0.22$. The discrepancy is substantially larger than the observed scatter in the Faber-Jackson relation ($\sim 0.5$ mag). While it is not clear what causes the difference, a possible explanation is an interaction with nearby structure which can strip the outer part of the galaxy mass and reduce the Einstein radius without changing the overall luminosity of the galaxy (e.g., Treu et al. 2008). However, the is no obvious companion galaxy at $z \sim 0.373$ around galaxy G, and no obvious signature of interaction in the galaxy images. Again,

extensive spectroscopy of galaxies in the field to study structure around the lens redshift might help to resolve this issue.

## 6 SUMMARY

We have presented the discovery of a new four-image lensed quasar SDSS J1330+1810 ($z_s = 1.393$). This source was selected as a lens candidate by the SQLS due to its extended morphology. Our observations in optical and near-infrared indicate that it is a typical fold-type quadruple lens, with a maximum separation between images of $1\farcs76$. From the spectrum we measured a lens redshift of $z_l = 0.373$. Standard simple elliptical mass models fit the data well, including the flux ratios, implying no evidence for substructure. The mass modelling suggests an important contribution of the external shear, probably from a nearby bright galaxy. There is also a foreground group of galaxies whose centre is $\sim 120''$ from the lens. The lens galaxy is $\sim 1$ mag brighter than predicted by mass modelling.

Thus far the SQLS has discovered 31 lensed quasars including SDSS J1330+1810[3], of which 5 are quadruple lenses (e.g., Inada et al. 2003; Kayo et al. 2007). The low fraction of quadruple lenses may imply that the faint end slope of the quasar optical luminosity function is shallow, although it is marginally consistent with standard theoretical expectations (Oguri 2007b). The SQLS has completed $\sim 2/3$ of its survey, implying that a few more quadruple lenses will be discovered by the completion of the survey.

## ACKNOWLEDGMENTS

We thank Paul Schechter for his help of the Magellan observation. This work was supported in part by Department of Energy contract DE-AC02-76SF00515 and RIKEN DRI Research Grant. J. A. B. acknowledges support from US NSF grant AST-0206010. I. K. acknowledges support from the JSPS Research Fellowships for Young Scientists and Grant-in-Aid for Scientific Research on Priority Areas No. 467. M. A. S. acknowledges support of NSF grant AST-0707266.

Funding for the SDSS and SDSS-II has been provided by the Alfred P. Sloan Foundation, the Participating Institutions, the National Science Foundation, the U.S. Department of Energy, the National Aeronautics and Space Administration, the Japanese Monbukagakusho, the Max Planck Society, and the Higher Education Funding Council for England. The SDSS Web Site is http://www.sdss.org/.

The SDSS is managed by the Astrophysical Research Consortium for the Participating Institutions. The Participating Institutions are the American Museum of Natural History, Astrophysical Institute Potsdam, University of Basel, University of Cambridge, Case Western Reserve University, University of Chicago, Drexel University, Fermilab, the Institute for Advanced Study, the Japan Participation Group, Johns Hopkins University, the Joint Institute for Nuclear Astrophysics, the Kavli Institute for Particle Astrophysics and Cosmology, the Korean Scientist Group, the Chinese Academy of Sciences (LAMOST), Los Alamos National Laboratory, the Max-Planck-Institute for Astronomy (MPIA), the Max-Planck-Institute for Astrophysics (MPA), New Mexico State University, Ohio State University, University of Pittsburgh, University of Portsmouth, Princeton University, the United States Naval Observatory, and the University of Washington.

This publication makes use of data products from the Two Micron All Sky Survey, which is a joint project of the University of Massachusetts and the Infrared Processing and Analysis Center/California Institute of Technology, funded by the National Aeronautics and Space Administration and the National Science Foundation.

[3] The current status of the survey is summarised at http://www-utap.phys.s.u-tokyo.ac.jp/~sdss/sqls/

## REFERENCES

Adelman-McCarthy J. K., et al., 2007, ApJS, 172, 634
Adelman-McCarthy J. K., et al., 2008, ApJS, 175, 297
Auger M. W., Fassnacht C. D., Abrahamse A. L., Lubin L. M., Squires G. K., 2007, AJ, 134, 668
Blanton M. R., Lin H., Lupton R. H., Maley F. M., Young N., Zehavi I., Loveday J., 2003, AJ, 125, 2276
Cabanac R. A., et al., 2007, A&A, 461, 813
Chae K.-H., 2003, MNRAS, 346, 746
Chiba M., 2002, ApJ, 565, 17
Csabai I., et al., 2003, AJ, 125, 580
Dalal N., Kochanek C. S., 2002, ApJ, 572, 25
Eisenstein D. J., et al., 2001, AJ, 122, 2267
Faber S. M., Jackson R. E., 1976, ApJ, 204, 668
Falco E. E., et al., 1999, ApJ, 523, 617
Fassnacht C. D., Lubin L. M., 2002, AJ, 123, 627
Fukugita M., Ichikawa T., Gunn J. E., Doi M., Shimasaku K., Schneider D. P., 1996, AJ, 111, 1748
Gunn J. E., et al., 1998, AJ, 116, 3040
Gunn J. E., et al., 2006, AJ, 131, 2332
Hogg D. W., Finkbeiner D. P., Schlegel D. J., Gunn J. E., 2001, AJ, 122, 2129
Huterer D., Keeton C. R., Ma C.-P., 2005, ApJ, 624, 34
Inada N., et al., 2003, AJ, 126, 666
Inada N., et al., 2008, AJ, 135, 496
Ivezić Ž., et al., 2004, AN, 325, 583
Kayo I., et al., 2007, AJ, 134, 1515
Keeton C. R., Kochanek C. S., Seljak U., 1997, ApJ, 482, 604
Keeton C. R., Christlein D., Zabludoff A. I., 2000, ApJ, 545, 129
Keeton C. R., 2003, ApJ, 584, 664
Landolt A. U., 1992, AJ, 104, 340
Mao S., Schneider P., 1998, MNRAS, 295, 587
Martini P., Persson S. E. Murphy D. C., Birk C., Shectman S. A., Gunnels S. M., Koch E., 2004, Proc. SPIE, 5492, 1653
Metcalf R. B., Madau P., 2001, ApJ, 563, 9
Momcheva I., Williams K., Keeton C., Zabludoff A., 2006, ApJ, 641, 169
Oguri M., 2007a, ApJ, 660, 1
Oguri M., 2007b, NJPh, 9, 442
Oguri M., Keeton C. R., Dalal N., 2005, MNRAS, 364, 1451
Oguri M., et al., 2006, AJ, 132, 999
Oguri M., et al., 2008, AJ, 135, 512
Padmanabhan N., et al., 2008, ApJ, 674, 1217

Peng C. Y., Ho L. C., Impey C. D., Rix H.-W., 2002, AJ, 124, 266
Petrosian V., 1976, ApJ, 209, L1
Pier J. R., Munn J. A., Hindsley R. B., Hennessy G. S., Kent S. M., Lupton R. H., Ivezić Ž., 2003, AJ, 125, 1559
Richards G. T., et al., 2002, AJ, 123, 2945
Rusin D., Tegmark M., 2001, ApJ, 553, 709
Rusin D., et al., 2003, ApJ, 587, 143
Schechter P. L., Wambsganss J., 2002, ApJ, 580, 685
Schneider D. P., et al., 2007, AJ, 134, 102
Shin M.-S., Strauss M. A., Oguri M., Inada N., Falco E. E., Broadhurst T., Gunn J. E., 2008, AJ, 136, 44
Skrutskie M. F., et al., 2006, AJ, 131, 1163
Smith J. A., et al., 2002, AJ, 123, 2121
Suyu S. H., Blandford R. D., 2006, MNRAS, 366, 39
Treu T., Gavazzi R., Gorecki A., Marshall P. J., Koopmans L. V. E., Bolton A. S., Moustakas L. A., Burles S., 2008, arXiv:0806.1056
Tucker D. L., et al., 2006, AN, 327, 821
Williams K. A., Momcheva I., Keeton C. R., Zabludoff A. I., Lehár J., 2006, ApJ, 646, 85
York D. G., et al., 2000, AJ, 120, 1579